Title

STRANGE-PARTICLE PRODUCTION FROM n+p INTERACTIONS IN THE c.m. ENERGY RANGE 1820 TO 2090 MeV

Authors

Hanson, P.
Kalmus, G.E.
Louie, J.

Publication Date

1970-07-01

Submitted to Physical Review

UCRL-19776
Preprint

c. 2

STRANGE-PARTICLE PRODUCTION FROM $\pi^+ p$ INTERACTIONS IN THE c.m. ENERGY RANGE 1820 TO 2090 MeV

P. Hanson, G. E. Kalmus, and J. Louie

July 1970

AEC Contract No. W-7405-eng-48

LAWRENCE RADIATION LABORATORY
UNIVERSITY of CALIFORNIA BERKELEY

UCRL-19776

c. 2

DISCLAIMER

UCRL-19776

STRANGE-PARTICLE PRODUCTION FROM $\pi^+ p$ INTERACTIONS IN THE c.m. ENERGY RANGE 1820 TO 2090 MeV*

P. Hanson, G. E. Kalmus, and J. Louie†

Lawrence Radiation Laboratory
University of California
Berkeley, California 94720

July 1970

ABSTRACT

Data at nine π^+ momenta are presented in the following three-body final states: $\Sigma^+K^+\pi^0$, $\Sigma^+K^0\pi^+$, $\Sigma^0K^+\pi^+$, $\Lambda K^+\pi^+$, $pK^+\bar{K}^0$. The data consist of cross sections, Dalitz plots, and angular distributions for the quasi-two-body final state $Y^{*+}(1385)\,K^+$. In the channel $Y^{*+}(1385)\,K^+$ the production and Y^* decay distributions are compared with the predictions of Stodolsky and Sakurai.[1]

I. INTRODUCTION

Data are presented from an exposure of $\pi^+ p$ taken in the Lawrence Radiation Laboratory 25-inch and 72-inch hydrogen bubble chambers at the Bevatron. Nine π^+ momenta (1.28, 1.34, 1.41, 1.43, 1.55, 1.63, 1.68, 1.77, and 1.84 GeV/c) were used. Discussion treats results obtained in the three-body final states

$$\pi^+ p \rightarrow \Sigma^+K^+\pi^0 , \quad (1)$$

$$\rightarrow \Sigma^+K^0\pi^+ , \quad (2)$$

$$\rightarrow \Lambda K^+\pi^+ , \quad (3)$$

$$\rightarrow \Sigma^0K^+\pi^+ , \quad (4)$$

$$\rightarrow pK^+\bar{K}^0 . \quad (5)$$

Data and analysis of the channel $\pi^+ p \rightarrow \Sigma^+K^+$ have been presented elsewhere.[2]

II. EXPERIMENTAL PROCEDURE

A. Exposure

All together, 783 000 pictures were taken at six momenta in the LRL 25-inch bubble chamber and 140 000 pictures at three momenta in the LRL 72-inch bubble chamber. The exposures at each energy varied in size from 1 to 2.5 events/microbarn. Details of the exposures are given in Table I. The momentum bite of the beam was between ± 0.8 and ± 1.0% at the various momenta.

B. Scanning

The film was scanned for two topologies: (a) two prongs, where one or both prongs have a kink and no visible recoil at the kink; and (b) two prongs with a V pointing to the vertex. Most of the film (more than 90%) was scanned twice. The combined scanning efficiency was found to be $\gtrsim 97\%$ for events eventually accepted as $\Sigma^+K^0\pi^+$ or $\Sigma^+K^+\pi^0$ and $\gtrsim 98\%$ for V^0 events.

C. Measuring

All events found in either scan were measured by use of the COBWEB on-line Frankenstein system. Any event not fitting with a reasonable χ^2 one of the hypotheses [(1)-(5)] or $\pi^+ p \rightarrow \Sigma^+K^+$ was remeasured. Candidates for hypotheses (1) and (2) that failed again to

fit satisfactorily were measured a third time. Any events that still did not fit were examined by a physicist to determine the cause of the failure.

D. Kinematic Fittings

1. V^0 Events

Events of the type two-prong plus V^0 were constrained to the hypotheses

$$\pi^+ p \to \Lambda K^+ \pi^+, \quad \Lambda \to \pi^- p, \qquad (3a)$$

$$\pi^+ p \to \Sigma^0 K^+ \pi^+, \quad \Sigma^0 \to \gamma \Lambda, \quad \Lambda \to \pi^- p, \qquad (4a)$$

$$\pi^+ p \to \bar{K}^0 K^+ p^+, \quad K^0 \to \pi^+ \pi^-. \qquad (5a)$$

Events were constrained to reactions (3a) and (5a) by using (a) a simultaneous two-vertex 7c fit; (b) a 1c fit at the production vertex (with the V^0 not used); and (c) a one-vertex 3c fit at the V^0 vertex. The two outgoing prongs at the first vertex were tried as $K^+\pi^+$ and π^+K^+ in turn and the V^0 was tried as $p\pi^-$ and $\pi^+\pi^-$. Only events that made the two-vertex fit were eventually accepted. Events were constrained to reaction (4) by using (a) a three-vertex 5c fit where the Σ^0 decay vertex is coincident with the production vertex; (b) a 1c fit at the production vertex (ignoring the V^0); and (c) a one-vertex 3c fit at the V^0 decay vertex.

2. Σ^+ Events

$$\pi^+ p \to \Sigma^+ K^+ \pi^0, \quad \Sigma^+ \to p\pi^0 \text{ or } \pi^+ n \qquad (1)$$

$$\to \Sigma^+ \pi^+ K^0, \quad \Sigma^+ \to p\pi^0 \text{ or } \pi^+ n \qquad (2)$$

The above two reactions were constrained in the following way when the $\Delta p/p$ (measured) of the Σ^+ was less than 0.5:

(a-1) A simultaneous two-vertex 2c fit was made.

(b-1) A single-vertex 1c fit was made at the first vertex.

When the Σ^+ was so short that $\Delta p/p > 0.5$, then

(a-2) a 0c calculation was performed at the Σ^+ decay vertex to obtain the Σ^+ momentum. This, in general, gave two solutions for each of the Σ^+ decay modes ($\pi^+ n$ and $p\pi^0$). These calculated values for the Σ^+ momentum were then used for the two-vertex fit (the Σ^+ momentum at the first vertex was corrected for the dE/dx loss).

(b-2) a 0c calculation of the Σ^+ momentum was made at the first vertex. The mass permutations (1) and (2) as well as the reaction $\pi^+ p \to \Sigma^+ K^+$ ($p\pi^0$ or $\pi^+ n$) were tried for each event (see Ref. 2 for a discussion of this reaction). How ambiguities were resolved between the various channels is discussed in the next section.

E. Resolution of Ambiguities

1. V^0 Events

There was essentially no problem in resolving reaction (3) from (5) nor (4) from (5). In the cases in which the V^0 fitted a Λ or K^0 or both (which were rare) the fit at the first vertex insured a complete separation.

Difficulty, however, was experienced in completely separating (3) from (4). Approximately 10% of events that fitted (3) also fitted (4) (with a reasonable χ^2) and 50% of events that fitted (4) also fitted (3). In other words, about 90% of the events that fitted either (3) or (4) or both were uniquely allocated by kinematic fitting. There were typically 4.3 times as many events per energy fitting (3) uniquely than either fitted (4) uniquely or were

ambiguous between the two. Thus, from the point of view of obtaining a channel cross section, the correct assignment of events was far more important for the $\Sigma^0 K^+ \pi^+$ channel than for the $\Lambda K^+ \pi^+$ channel. To a lesser extent the same is true for angular distributions, mass plots, etc. The following procedure was used to assign events, keeping in mind our philosophy that a clean, unbiased sample of events was needed in the $\Lambda K^+ \pi^+$ channel, whereas, because of lack of statistics, the main interest in the $\Sigma^0 K^+ \pi^+$ channel was the cross section.

Of the 87 events that fitted both (3) and (4), about 35% were resolved on the basis of the ionization of the outgoing tracks (π^+ and K^+) at the first vertex (i.e., in going from (3) to (4) the mass assignments of these two tracks were switched). A further 30% of the ambiguous events, although having both kinematic χ^2's acceptable, had one χ^2 probability much greater than the other (by a factor of at least 5). The remaining 35% of the events were essentially unresolvable and were assigned approximately in the ratio $\Lambda^0/\Sigma^0 = 2$, after considering all the kinematic and ionization factors both before and after constraint. Thus of the 32 events in this last class, 21 events (out of a total of 790 events) were assigned to the Λ hypothesis, and 11 events (out of a total of 97 events) were assigned to the Σ^0 hypothesis.

2. Σ^+ Events

The following topologies and mass permutations are involved in these events:

$$\pi^+ p \rightarrow \Sigma^+ K^+ \pi^0 \quad (1)$$
$$\rightarrow p\pi^0 \quad (1a)$$
$$\rightarrow \pi^+ n \ , \quad (1b)$$

$$\pi^+ p \rightarrow \Sigma^+ K^0 \pi^+ \quad (2)$$
$$\rightarrow p\pi^0 \quad (2a)$$
$$\rightarrow \pi^+ n \ , \quad (2b)$$

$$\pi^+ p \rightarrow \Sigma^+ K^+ \quad (6)$$
$$\rightarrow p\pi^0 \quad (6a)$$
$$\rightarrow \pi^+ n \ . \quad (6b)$$

The events that were found to be kinematically ambiguous between (6) and (1) or (2) were examined for ionization. In addition, on the assumption that they were of topology (6), their production angle was plotted. It was found that these events (which accounted for 5 to 10% of all the $\pi^+ p \rightarrow \Sigma^+ K^+$ events) were in all cases consistent with hypothesis (6), both with regard to ionization when this was a factor [e.g., when the ambiguity was between (2a) and (6b)] and also with regard to their production angles, which were distributed in a manner completely consistent with the angular distributions of the unambiguous sample. This second argument is used only to strengthen our belief that false events are much less likely to fit when there are 4 (or 5) constraints than when there is only 1 (or 2).

Events that had a good χ^2 to the two-vertex fit for reaction (6) were therefore assumed to be of this type even if they also fitted (1) or (2).

We are then left with the ambiguities between (1) and (2). These are of three types: (a) those between (1a) and (2a) [or (1b) and (2b)], i.e., different production processes but the same Σ^+ decay mode; (b) those between (1a) and (1b) [or (2a) and (2b)], i.e., same production process but different Σ^+ decay modes; and (c) those between (1a) and (2b) [or (1b) and (2a)], i.e., different production processes and different Σ^+ decay modes. In essentially all cases, ambiguities of the types

(b) and (c) were resolved by ionization of the charged track from the Σ^+ decay. Ambiguities of type (a)--which typically account for about 25% of the events (1) and (2)--were, in general, resolved by an examination of all the tracks on the scan table. In all but a very few cases [less than 5% of events fitting (1) or (2)] a definite preference for one of the hypotheses over the other was found by these means.

III. DATA AND RESULTS

A. Acceptance Criteria

1. V^0 Events

Table II shows the number of events found at each energy in the various channels that satisfy the following criteria:

(a) Beam track is acceptable.

(b) V^0 decay vertex is more than 0.8 cm from production vertex.

(c) Both the production and decay vertices are within their respective fiducial volumes.

(d) V^0 lives less than three mean lives.

Since cuts (b) and (c) are momentum dependent, each event was weighted to take these as well as (d) into account.

2. Σ^+ Events

Table II shows the number of events found at each energy in the two channels that satisfy the following cuts:

(a) Beam track is acceptable.

(b) Σ^+ is > 0.3 cm long and does not live more than three mean lives.

(c) The Σ^+ decay angle (lab) is > 5 deg (> 10 deg for 72-inch chamber film.

(d) The event is within the fiducial volume.

These cuts are identical to those imposed on the $\pi^+p \to \Sigma^+K^+$ events described in Ref. 2. Since cuts (b) and (c) are Σ^+ momentum dependent, each event was weighted to take into account those two cuts as well as the possibility that the Σ^+ left the chamber. For a detailed discussion of how the values of these cuts were determined, see Ref. 2. Since the Σ^+ momentum range of these events is not very different from that of the $\pi^+p \to \Sigma^+K^+$ events, the cuts determined for those events should still be valid. It should be noted that because of the rather small number of events in these three-body final states both the $\Sigma^+ \to \pi^+n$ and $\Sigma^+ \to p\pi^0$ decay modes were used in the determination of the cross section.

B. $\pi^+p \to \Lambda K^+\pi^+$ Channel

1. Data

Table II and Fig. 1 show the cross section for this channel as a function of π^+ momentum. Also, on Fig. 1 is the cross section for $\pi^+p \to \Sigma^+K^+$ for comparison, obtained from Ref. 2.

Table III shows the cross section for $\pi^+p \to Y^*(1385)\,K^+$.

Figures 2a through f show the Dalitz plots and projections at all but our two lowest momenta, where there are not sufficient events to warrant this (the 1.41- and 1.43-GeV/c data have been combined). Figure 3 shows the Dalitz plot and projections for the three highest momenta (1.68, 1.77, and 1.84 GeV/c) combined. Figures 4a through f show the $\Lambda\pi^+$ mass-squared plots corresponding to fits 2a through f, where weighted events have been plotted. Figure 4e has a curve superimposed on it; this is the fit to the data using a Breit-Wigner form for the $Y^*(1385)$ and a constant matrix element for the background. Figure 5 shows the $\Lambda\pi^+$ mass-squared histogram for the highest three momenta combined (for weighted events).

Figures 6a through g show the production angular distribution for the reaction $\pi^+p \to Y^*(1385)\,K^+$ with $[Y^*(1385) \to \Lambda\pi^+]$ when the $Y^*(1385)$ has been defined as being all events with $1340 < M_{\Lambda\pi^+} < 1430$ MeV. Cos θ is defined as $(\hat{\pi}_{beam} \cdot \hat{K})/(|\hat{\pi}_{beam}||\hat{K}|)$ in the c.m. system, where $\hat{\pi}_{beam}$ and $\hat{K}$ are

unit vectors along the directions of these particles in the overall c.m. system.

Figures 7a through g show the $Y^*(1385)$ decay angular distribution in the Y^* center-of-mass system with respect to the production normal, i.e., $\cos\phi = (\hat{n}\cdot\hat{\pi}^+_{out})/(|\hat{n}||\hat{\pi}^+_{out}|)$, where $\hat{n} = (\hat{\pi}_{beam}\times\hat{K})/(|\hat{\pi}_{beam}\times\hat{K}|)$, and $\hat{\pi}_{out}$ is a unit vector along the outgoing π^+ direction in the $Y^*(1385)$ center-of-mass system.

2. Results

a. From Fig. 1. it can be seen that the cross section for $\pi^+p \to \Lambda K^+\pi^+$ rises steeply from threshold and appears to peak or level off at $\approx P_{\pi^+} = 1.75$ GeV/c. This is borne out by the data of Dagan et al.,[3] who obtain a cross section of 140 ± 30 μB at $P_{\pi^+} = 1.95$ GeV/c, and Foelshe et al.,[4] who obtain 190 ± 40 μb and 120 ± 30 μb at 1.76 and 2.08 GeV/c respectively. The value at $P_{\pi^+} = 1.76$ GeV/c is in excellent agreement with our own value at 1.77 GeV/c.

From the Dalitz plots and projections (Figs. 2 and 4) it can be seen that the channel is dominated by $Y^*(1385)$ production. The three highest momenta were examined in detail for evidence of any structure of the type reported by Pan and Forman[5] at a $\Lambda\pi^+$ mass of $\approx$ 1480 MeV. The $\Lambda\pi^+$ mass-squared plot is shown in Fig. 5. These three momenta are the only ones that are above threshold for the production of such an object. No statistically significant enhancement is seen, although there is a small excess of events in the region 2.13 to 2.21 $(GeV)^2$. However, it should be pointed out that our data consist of 337 unweighted events (420 weighted), compared with the 982 events of Pan and Forman. If we scale their enhancement by the ratio of the number of events, we would expect to see about 16 events above background in our weighted data. In the two boxes from 2.13 and 2.21 $(GeV)^2$ we have a total of 22 weighted events; this number is compatible with being due to background alone. The uncertainties in the shape of the background are clearly such that we cannot rule out an enhancement of the type seen by Pan and Forman. However, our data do not require any structure at a mass of $\approx$ 1480 MeV. It should be noted that "background" in this region would be enhanced by the presence of an N^* of mass $\approx$ 1660 MeV which decays, with a small branching ratio, into ΛK^+. However, this would not give a sharp peak.

We have also examined the polarization of the Λ with respect to the production plane as a function of the $\Lambda\pi^+$ mass. We find that the errors are so large in the mass region near 1480 MeV that no useful conclusion can be drawn [the error in αP for a bin of width 0.05 $(GeV)^2$ is typically ± 0.5]. In both the 1385 and 1480 MeV mass regions the data are consistent with zero polarization.

b. We have compared the Y^* production and decay distributions with two models:
(i) Stodolsky-Sakurai Model. The main assumptions of this model are well known and are illustrated in Fig. 8. The model makes the analogy between the ρ meson and the isovector part of the photon. Thus the lower vertex of Fig. 8a is assumed to be the same as the vertex in Fig. 8b. Thus the properties of the photoproduction amplitude of the Δ can be used to predict the amplitude for diagram 8a (assuming the $\rho \to \pi\pi$ vertex is known). This model has had some success at predicting amplitudes where ρ exchange is dominant. It was also suggested by Stodolsky and Sakurai that the same model might be valid for K^* exchange (Fig. 8d). The connection between the ρ and K^* (and Δ and Y^*) being via SU(3). The predictions of this model are that the form of the production angular distribution is given by $dN/d\cos\theta \propto (1-\cos^2\theta)/(t-M_{K^*})^2$, where θ has been defined earlier; t is the four-momentum transfer squared, $(p_\pi - p_K)^2$; and M_{K^*} is the mass of the K^*. The form of the decay angular distribution (with respect to

the production normal) is given by $dN/d\cos\phi \propto 1 + 3\cos^2\phi$, where ϕ has been defined earlier. These are shown as the solid curves on Figs. 6 and 7.

(ii) s-Channel model. In this we assume that the reaction proceeds through an intermediate $\Delta(1950)$, i.e., $\pi^+p \to \Delta(1950) \to Y^*(1385)K^+$, where the Δ decays via an $\ell = 3$ state (not the $\ell = 5$ state). The production distribution is of the form $dN/d\cos\theta \propto (294 - 2205\cos^2\theta + 7560\cos^4\theta - 5425\cos^6\theta)$, and the decay distribution is of the form $dN/d\cos\phi \propto (89 - 5\cos^2\phi)$.

These predictions are shown as the dotted curves on Figs. 6 and 7.

From Fig. 6 it can be seen that the Stodolsky-Sakurai model fits the production distributions, at all momenta, reasonably well, whereas the s-channel model predictions are inconsistent with the data. The Y^* decay distributions shown in Fig. 7 also qualitatively fit the Stodolsky-Sakurai model predictions at all momenta. The s-channel model also fits these data reasonably well at all but 1.55 and 1.63 GeV/c. One might have suspected the fit to be best here near the peak of the $\Delta(1950)$.

Davies et al.[6] have also found agreement between their production data, in the same channel, and the Stodolsky-Sakurai models.

C. $\pi^+p \to K^+\bar{K}^0p$ Channel

1. Data and results

Table II and Fig. 8 show the cross section for this channel. The number of events is clearly such that no useful result except for the cross section can be obtained.

D. $\pi^+p \to \Sigma^+K^+\pi^0$ Channel

1. Data

Table II and Fig. 9 show the cross section for this channel. These were obtained by using the weighted number of events for both decay modes of the Σ^+. As can be seen from Table II, there would be no disagreement had only the $\Sigma^+ \to \pi^+n$ events been used.

Figures 11a and 11b show the Dalitz plot and projections for the data at 1.55 and 1.62 GeV/c combined and at 1.68, 1.77, and 1.84 GeV/c combined. Figures 12a and 12b show the $\Sigma^+\pi^0$ mass-squared plot for these two groups of momenta for weighted events.

2. Results

To investigate the enhancement seen by Pan and Forman at 1480 MeV in the $\Lambda\pi^+$ system and at 1465 MeV in the $\Sigma^+\pi^0$ and $\Sigma^0\pi^+$ system,[7] we examine Fig. 12. Our data show less structure than theirs; in Fig. 12a the $Y^*(1385)$ is seen, whereas in Fig. 12b there is only a rather small indication of it. In both figures there is a high bin centered at 2.12 $(GeV)^2$ (1.455 MeV). However, at the higher momenta (Fig. 12b) this is very narrow ($\lesssim$ 20 MeV), and consists of only 12 events unweighted (23 weighted). The curves on Fig. 12 show the best fit assuming the production of a $Y^*(1385)$ on top of phase space. It can be seen that the high bin in Fig. 12b is only 2 standard deviations above the curve, and thus the data is not incompatible with the curve. It should be noted that Fig. 12b contains 144 weighted events (110 unweighted) to be compared to the 169 events in this channel in Ref. 7.

The polarization of the events with $\Sigma^+ \to p\pi^0$ was calculated as a function of $\Sigma^+\pi^0$ mass. However, the errors are so large that the results are valueless [the error in $\alpha\bar{P}$ is $\approx$ 0.5 for a box of width 0.05 $(GeV)^2$].

Finally, an estimate of the cross section $\pi^+p \to Y^*(1385)K^+; Y^*(1385) \to \Sigma^+\pi^0$ for two batches of data can be made.

We obtain at 1.55 and 1.63 GeV/c, 10 ± 5 μb; and at 1.68, 1.77, and 1.84 GeV/c, 5 ± 3 μb.

E. $\pi^+ p \rightarrow \Sigma^0 K^+ \pi^+$ Channel

1. Data

Table II and Fig. 13 show the cross section for this channel. The errors on the cross section are due both to statistics and to the possibility of a bias in assigning overlap events between the $\Sigma^0 K^+ \pi^+$ and $\Lambda K^+ \pi^+$ channels. Figures 14a, b show the Dalitz plots and projections for the 1.55- and 1.63-GeV/c data combined and the 1.68-, 1.77-, and 1.84-GeV/c data combined.

2. Results

Figures 15a, b show the $\Sigma^0 \pi^+$ mass-squared plots for weighted events for the two sets of data. Very little can be said with such limited statistics. There is evidence in Fig. 15b, which contains 59 weighted events (48 unweighted), that the $Y^*(1385)$ is present.

Figure 16a shows the sum of Figs. 12b and 15b (203 weighted events), and can now be compared more directly with the data of Forman and Pan shown in Fig. 16b. The two sets of data are compatible, although Forman and Pan's enhancement is at higher mass than the "peak" in our data. Our data, however, are also adequately fitted by phase space (weighted sum at the three beam momenta) times a Breit-Wigner resonance for the $Y^*(1385)$.

F. $\pi^+ p \rightarrow \Sigma^+ \pi^+ K^0$

1. Data and Results

Table II and Fig. 10a show the cross section for this channel. The cross section was obtained by using only the events in which the K^0 did not materialize (and correcting for those in which it did). Both decay modes of the Σ^+ were used. Figure 17 shows the Dalitz plot and projections for the sum of the 1.62-, 1.68-, 1.77-, and 1.84-GeV/c data. No structure is seen in the $\Sigma^+ \pi^+$ mass plot. Fig. 18, which, had it been present, would indicate an "exotic" state.

IV. DISCUSSION

No definite conclusion can be reached as to the presence of a $Y^*(1470)$ of the type seen by Pan and Forman. Both the $\Lambda \pi^+ K^+$ and $\Sigma^+ \pi^0 K^+$ mass plots (Figs. 5 and 16) have small enhancements (over phase space) in this region (the $\Sigma^+ \pi^0$ enhancement being at a very low mass, $\approx$ 1455). However, in both cases the effects are less significant than those seen by Pan and Forman, even taking into account our lower statistics. In each case a distortion of phase space (perhaps due to an N^* in the ΛK^+ system) would reduce the significance of the enhancement even further. It should be emphasized, however, that our data are quite consistent with theirs.

We find good agreement between the predictions of the Stodolsky-Sakurai model and the Y^* production and decay (with respect to the production normal) distributions. Not surprisingly, there is poor agreement with the s-channel model, at all momenta.

Thus it would appear that the ρ-photon analogy can be extended to a K^*-photon analogy. We have, in addition examined the Trieman-Yang angle for the $Y^*(1385)$ decay. This is shown in Fig. 19 (for three highest momenta), the curve being the Stodolsky-Sakurai prediction. It can be seen that the agreement is quite reasonable. It should be noted that the Y^* decay angle (with respect to the production normal) and the Trieman-Yang angle are not independent. We thus conclude that the K^*-photon analogy is reasonable, at least as a qualitative description of the data.

Finally, the measured cross sections of the three channels $\Sigma^+ K^+ \pi^0$, $\Sigma^0 K^+ \pi^+$, and $\Sigma^+ K^0 \pi^+$ enable us to check the prediction of charge independence which states that there should be a "triangle inequality" between $(2\sigma_{\Sigma^+ K^+ \pi^0})^{1/2}$, $(2\sigma_{\Sigma^0 K^+ \pi^+})^{1/2}$, and $(\sigma_{\Sigma^+ K^0 \pi^+})^{1/2}$, where σ is the cross section

for the appropriate channel--i.e., the sum of any two of these must be greater than or equal to the third. Table IV gives these three quantities, and it can be seen that charge independence is not violated at any of the momenta.

FOOTNOTES AND REFERENCES

*Work done under auspices of the U. S. Atomic Energy Commission.

†Present address: Brookhaven National Laboratory, Upton, Long Island, New York.

1. L. Stodolsky and J. J. Sakurai, Phys. Rev. Letters 11, 90 (1963). See also L. Stodolsky, Phys. Rev. 134, B1099 (1964).
2. G. E. Kalmus, G. Borreani, and J. Louie (UCRL-19735, March 1970). Submitted to Phys. Rev., and G. E. Kalmus, G. Borreani, and J. Louie (UCRL-19777, July 1970), submitted to Phys. Rev.
3. S. Dagan, Z. Ming Ma, J. W. Chapman, L. R. Fortney, and E. C. Fowler, Phys. Rev. 161, 1384 (1967).
4. H. W. J. Foelshe, A. Lopez-Cepero, C. Y. Chien, and H. L. Kraybill, submitted to XIIth International Conference on High Energy Physics, Dubna, 1964 (unpublished).
5. Y. L. Pan and F. L. Forman, Phys. Rev. Letters 23, 806 (1969).
6. D. W. Davies, M. A. Abolins, O. I. Dahl, J. S. Danburg, P. L. Hoch, J. Kirz, D. H. Miller, and R. K. Rader, Phys. Rev. (to be published).
7. Y. L. Pan and F. L. Forman, Phys. Rev. Letters 23, 808 (1969).

Table I. Exposure parameters.

Momentum (GeV/c)	Energy, c.m. (GeV/c)	Number of pictures (1000)	Chamber (in.)	Cross section for one event (μb) (approx.)
1.28	1.823	127	25	0.6
1.34	1.851	52	72	0.4
1.41	1.886	130	25	0.6
1.43	1.896	41	72	0.5
1.55	1.955	121	25	0.8
1.62	1.992	164	25	0.5
1.68	2.016	47	72	0.5
1.77	2.057	122	25	0.7
1.84	2.089	119	25	0.9

TABLE II. Channel cross sections.

π^+ Momentum (GeV/c)	$\Lambda^0 K^+ \pi^+$ Events (Unwted)	Events (Wted)	Cross section (μb)	$pK^+\bar{K}^0$ Events (Unwted)	Events (Wted)	Cross section (μb)	$\Sigma^0 K^+ \pi^+$ Events (Unwted)	Events (Wted)	Cross section (μb)	$\Sigma^+ K^+ \pi^0$ Events (Unwted)	Events (Wted)	Cross section (μb)	$\Sigma^+ K^0 \pi^+$ Events (Unwted)	Events (Wted)	Cross section (μb)
1.28	3	3.8	$4.5^{+3.3}_{-1.6}$	← BELOW THRESHOLD →											
1.34	0	0	< 2 95% C.L.	BELOW THRESHOLD			0	0	< 2 95% C.L.	a 0	0	< 2 95% C.L.	a 1	1.4	$3^{+2.2}_{-1.2}$
										b 0	0		b 2	2.5	
1.41	18	24	25 ± 6	BELOW THRESHOLD			0	0	< 4 95% C.L.	a 3	3.9	$4^{+2.2}_{-1.6}$	a 0	0	< 4 95% C.L.
										b 1	1.3		b 0	0	
1.43	34	45	42 ± 12	BELOW THRESHOLD			2	2.3	2^{+2}_{-1}	a 5	6.7	6 ± 3	a 1	1.3	2^{+2}_{-1}
										b 3	3.8		b 1	1.2	
1.55	58	83	107 ± 16	1	1.5	$3.7^{+5.4}_{-1.9}$	6	7.6	10 ± 4	a 8	10.9	21 ± 6	a 5	6.3	14 ± 6
										b 9	11.4		b 3	3.8	
1.63	149	209	163 ± 16	1	1.3	$2^{+2.6}_{-1.4}$	12	14.4	11 ± 4	a 15	19.0	25 ± 6	a 11	14.0	25 ± 7
										b 18	22.7		b 11	14.2	
1.68	113	145	128 ± 13	3	4.4	$8^{+5.4}_{-2.7}$	18	20.7	18 ± 5	a 13	18.5	30 ± 6	a 9	12.2	24 ± 6
										b 15	18.5		b 10	12.4	
1.77	115	157	170 ± 17	6	7.7	17 ± 7	15	18.3	20 ± 7	a 14	17.8	40 ± 15	a 11	14.1	42 ± 14
										b 25	32.3		b 17	21.8	
1.84	80	109	162 ± 18	6	8.4	25 ± 10	15	19.9	30 ± 9	a 27	36.3	70 15	a 16	21.9	72 ± 16
										b 20	25.6		b 16	20.7	

a. $\Sigma^+ \to p\pi^0$; b. $\Sigma^+ \to \pi^+ n$

Table III.

Cross sections for $\pi^+ p \to Y^*(1385)\ K^+$ $(Y^* \to \Lambda\pi^+)$.

Beam momentum (GeV/c)	Y^*K^+ Cross section (μb)
1.41	25 ± 6
1.43	42 ± 12
1.55	95 ± 20
1.63	130 ± 20
1.68	100 ± 20
1.77	125 ± 25
1.84	140 ± 25

Table IV. Magnitudes of the three quantities needed for the "triangle inequality test" of charge independence.

Beam momentum (GeV/c)	$(\sigma_{\Sigma^+K^o\pi^+})^{\frac{1}{2}}$ $(\mu b)^{\frac{1}{2}}$	$(2\sigma_{\Sigma^+K^+\pi^o})^{\frac{1}{2}}$ $(\mu b)^{\frac{1}{2}}$	$(2\sigma_{\Sigma^oK^+\pi^+})^{\frac{1}{2}}$ $(\mu b)^{\frac{1}{2}}$
1.34	$1.7\ ^{+0.6}_{-0.4}$	< 2	< 2
1.41	< 2	$2.8\ ^{+0.7}_{-0.6}$	< 2.8
1.43	$1.4\ ^{+0.6}_{-0.4}$	$3.5\ ^{+0.8}_{-1.0}$	$2.0\ ^{+0.8}_{-1.0}$
1.55	$3.7\ ^{+0.8}_{-0.9}$	$6.5\ ^{+0.9}_{-1.0}$	$4.5\ ^{+0.8}_{-1.0}$
1.62	$5.0\ ^{+0.7}_{-0.8}$	$7.1\ ^{+0.8}_{-0.9}$	$4.7\ ^{+0.8}_{-0.9}$
1.68	$4.9\ ^{+0.6}_{-0.7}$	$7.7\ ^{+0.8}_{-0.8}$	$6.0\ ^{+0.8}_{-0.9}$
1.77	$6.5\ ^{+1.0}_{-1.2}$	$9.0\ ^{+1.1}_{-2.0}$	$6.3\ ^{+1.0}_{-1.3}$
1.84	$8.5\ ^{+0.9}_{-1.0}$	$11.8\ ^{+1.2}_{-1.4}$	$7.7\ ^{+1.1}_{-1.3}$

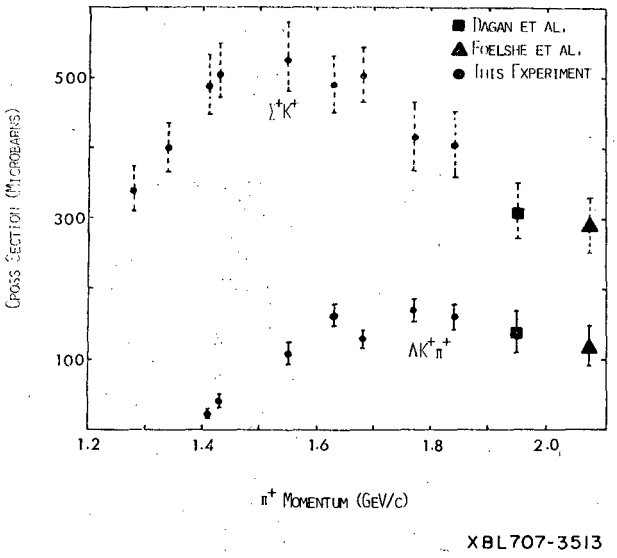

Fig. 1. Cross sections for the channels $\pi^+p \rightarrow \Lambda K^+\pi^+$ and $\pi^+p \rightarrow \Sigma^+K^+$.

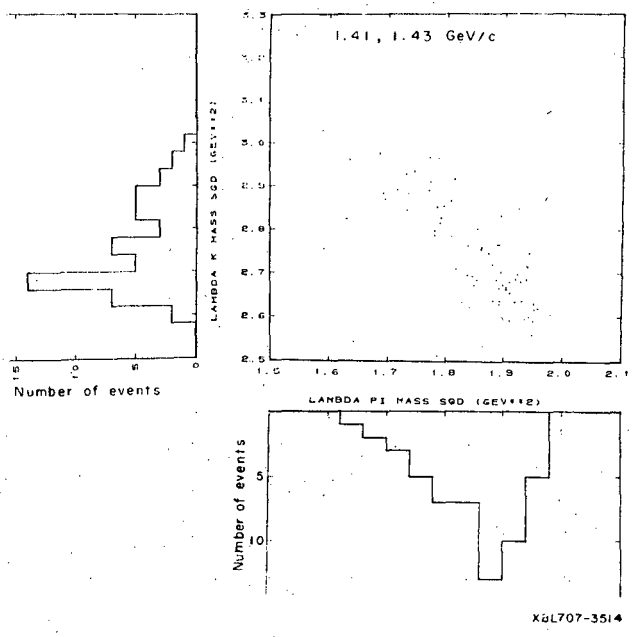

Fig. 2a

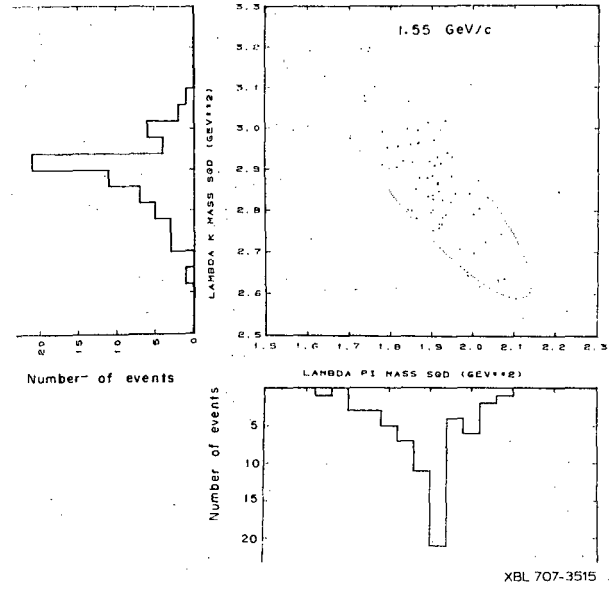

Fig. 2b

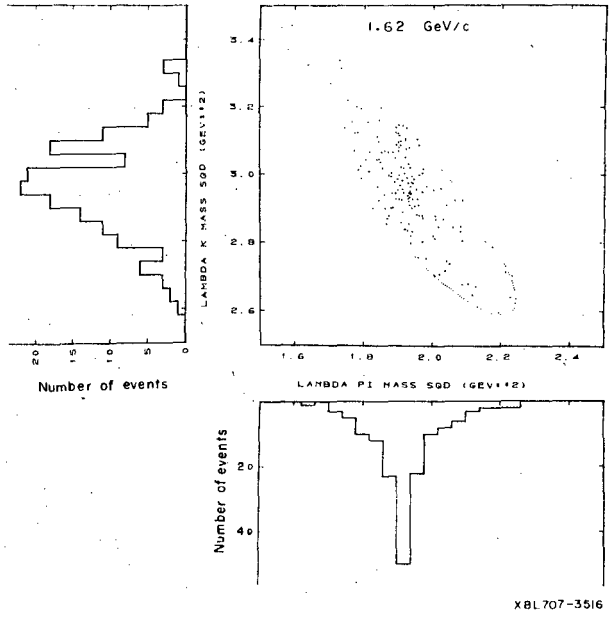

Fig. 2c

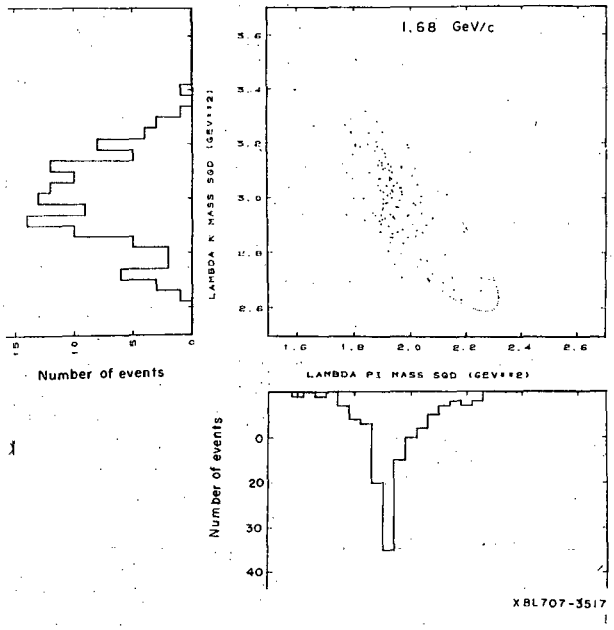

Fig. 2d

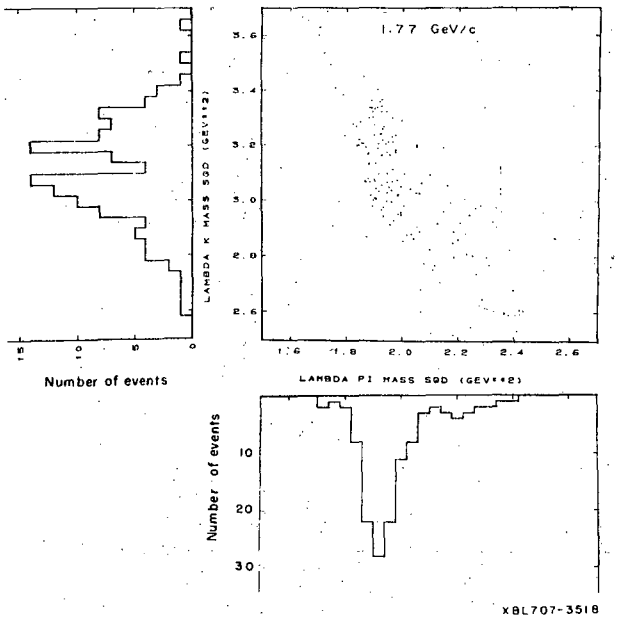

Fig. 2e

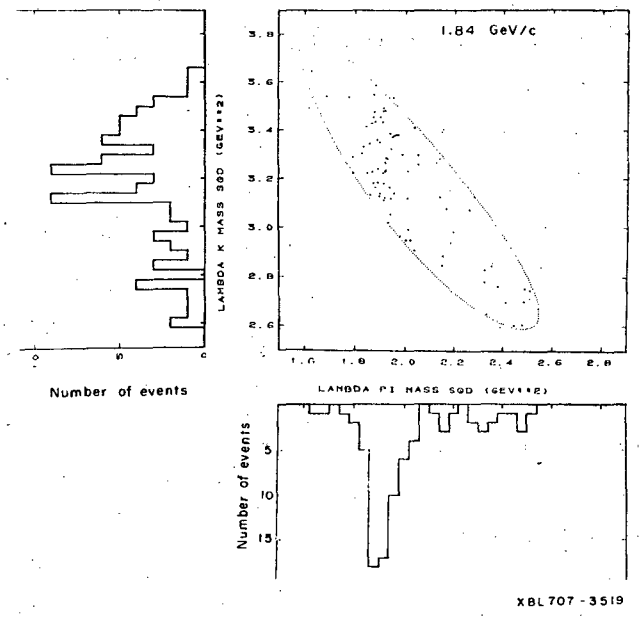

Fig. 2f

Fig. 2. Plots of ΛK^+ invariant mass squared versus $\Lambda\pi^+$ invariant mass squared, and histograms of the projections onto the two axes.

(a) π^+ momentum 1.41 and 1.43 GeV/c (the boundaries drawn are for the corresponding two c.m. energies)

(b) π^+ momentum 1.55 GeV/c.

(c) π^+ momentum 1.62 GeV/c

(d) π^+ momentum 1.68 GeV/c

(e) π^+ momentum 1.77 GeV/c

(f) π^+ momentum 1.84 GeV/c.

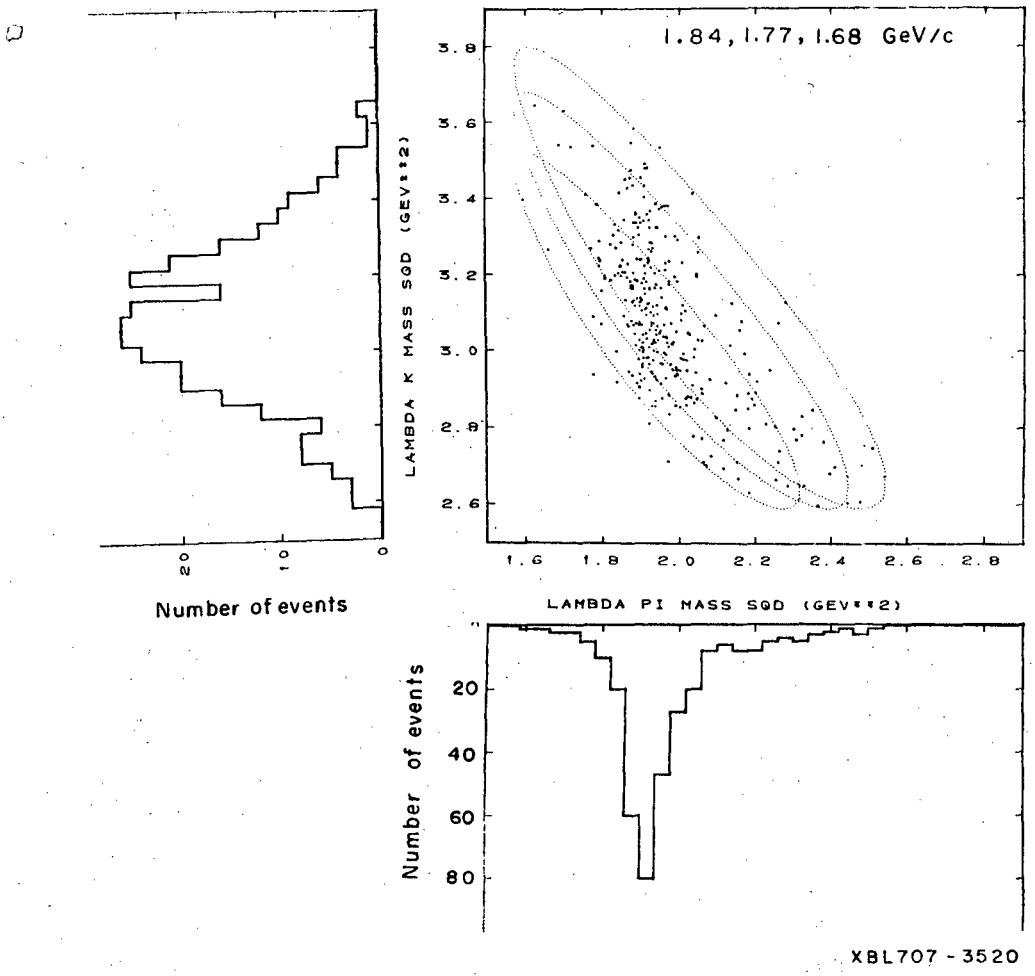

Fig. 3. Sum of 2d, 2e, and 2f.

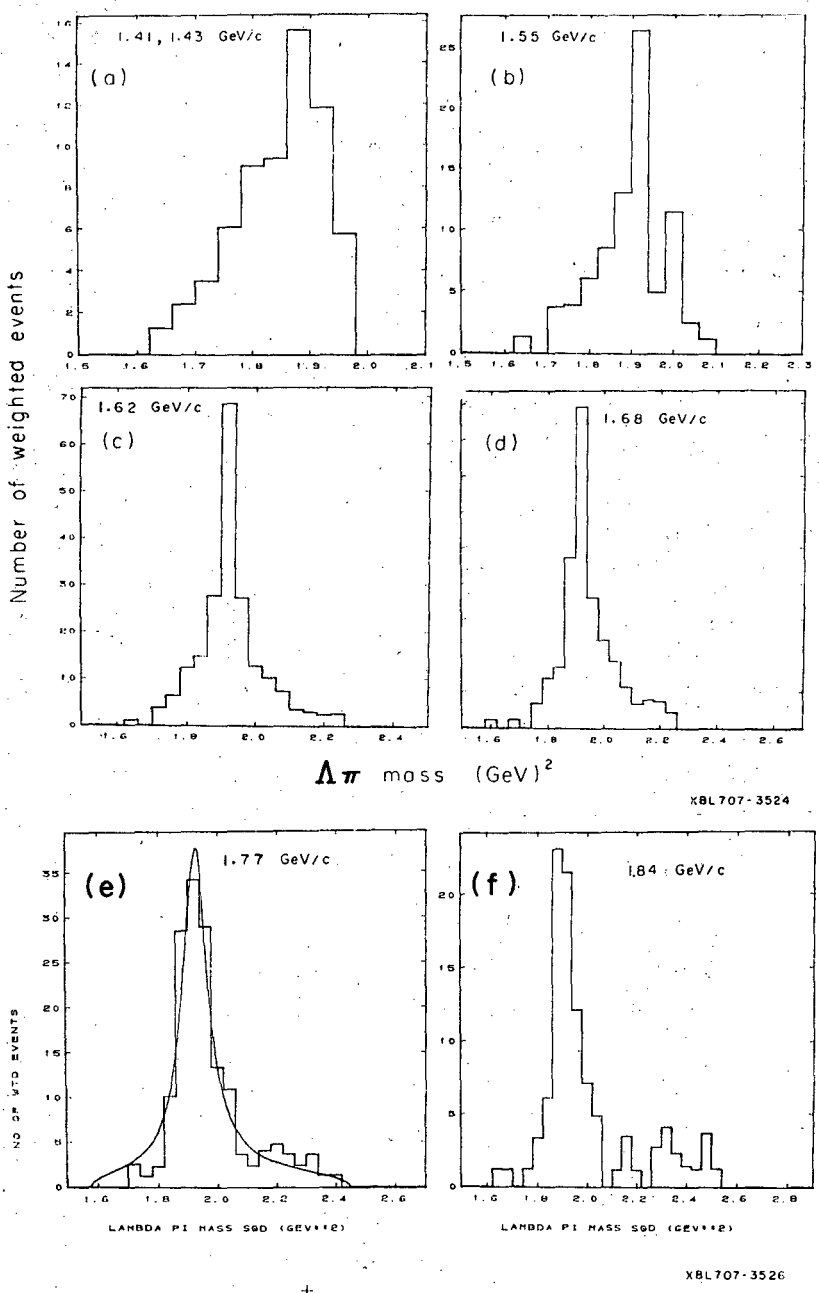

Fig. 4. $\Lambda\pi^+$ invariant-mass-squared histogram for weighted events.
(a) π^+ momentum 1.41 and 1.43 GeV/c
(b) π^+ momentum 1.55 GeV/c
(c) π^+ momentum 1.62 GeV/c
(d) π^+ momentum 1.68 GeV/c
(e) π^+ momentum 1.77 GeV/c. The curve is a Breit-Wigner [for $Y^*(1385)$] on top of phase space.
(f) π^+ momentum 1.84 GeV/c.

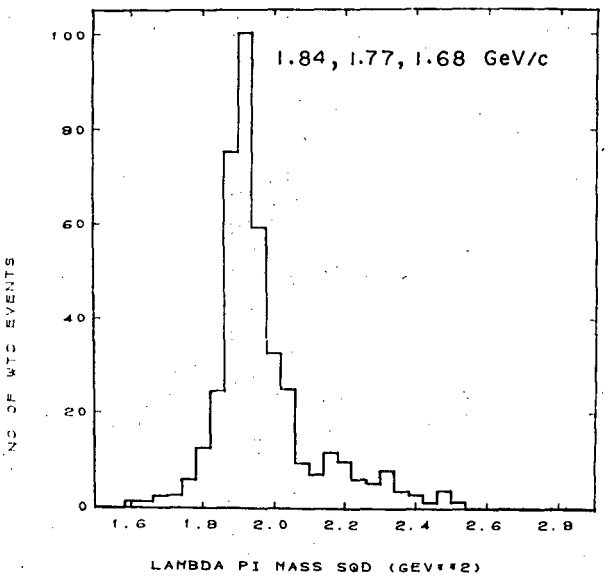

XBL707-3525

Fig. 5. Sum of 4d, 4e, and 4f.

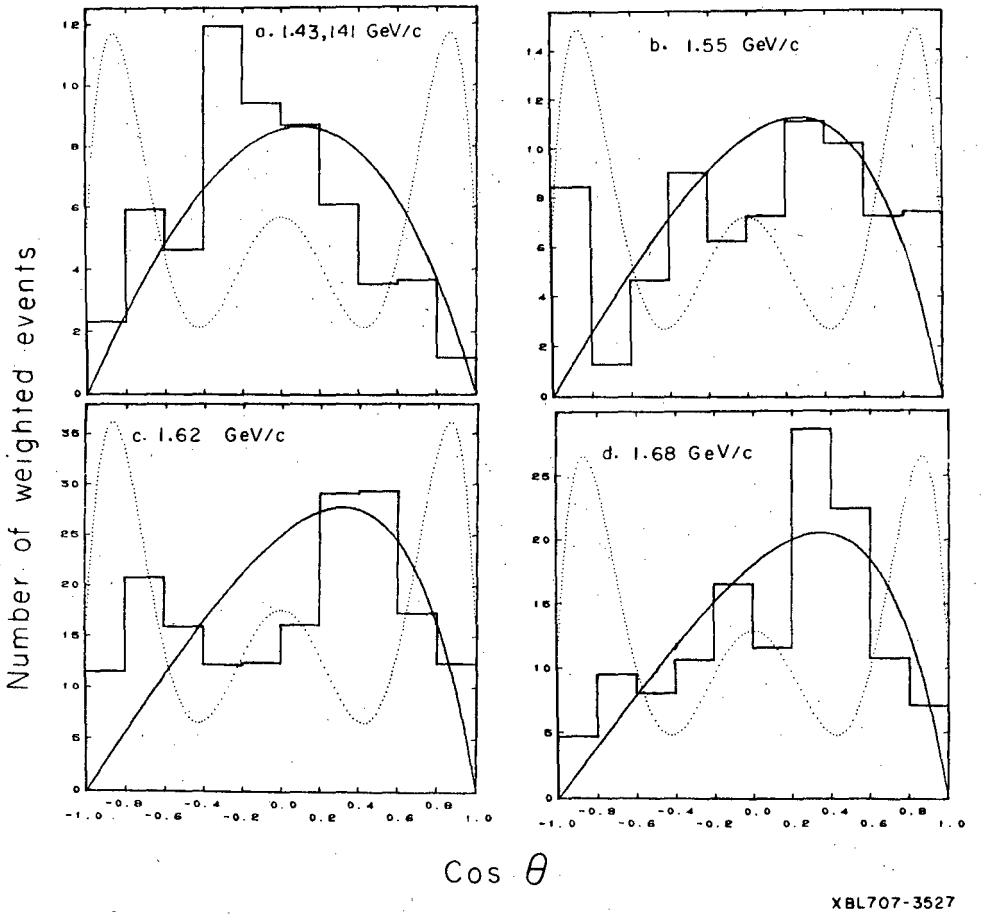

XBL707-3527

Fig. 6a-d

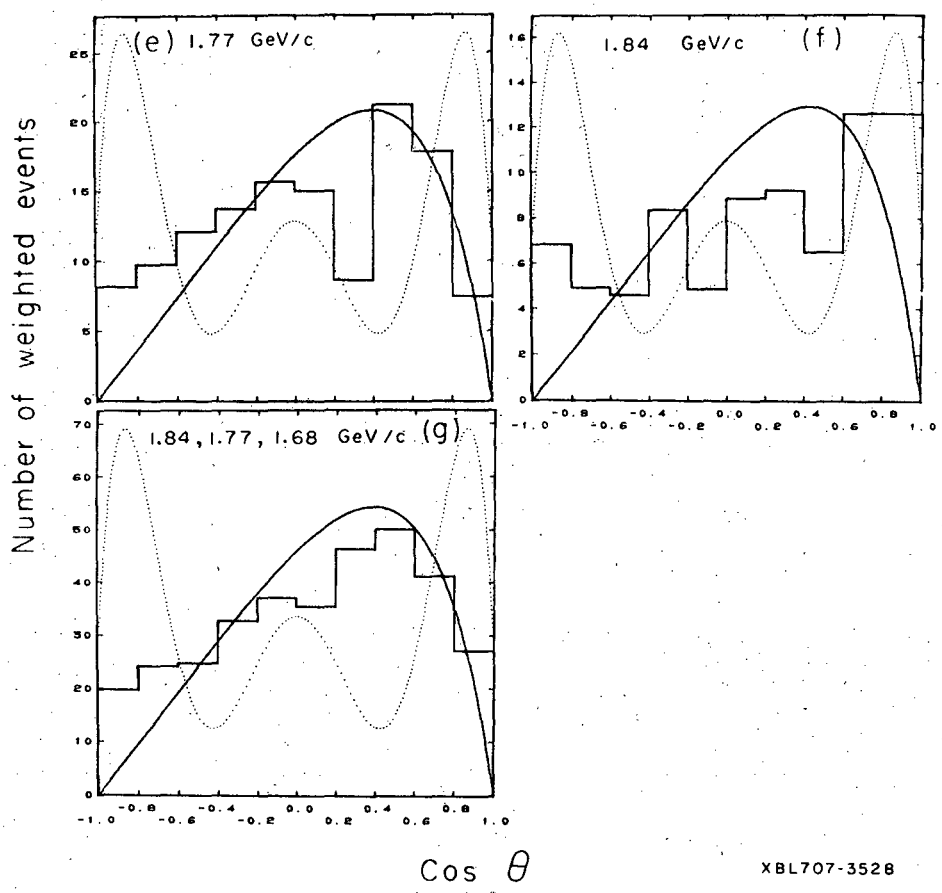

Fig. 6. Production angular distribution for the reaction $\pi^+ p \rightarrow Y^*(1385) K^+$. The full curve is the prediction of the Stodolsky-Sakurai model, the broken curve is the prediction assuming the reaction proceeds by $\pi^+ p \rightarrow \Delta(1950) \rightarrow Y^* K^+$ above the Δ decays via an $\ell = 3$ (not $\ell = 5$) state.

(a) π^+ momenta 1.41 and 1.43 GeV/c
(b) π^+ momenta 1.55 GeV/c
(c) π^+ momenta 1.62 GeV/c
(d) π^+ momenta 1.68 GeV/c
(e) π^+ momenta 1.77 GeV/c
(f) π^+ momenta 1.84 GeV/c
(g) π^+ momenta 1.68, 1.77, and 1.84 GeV/c combined.

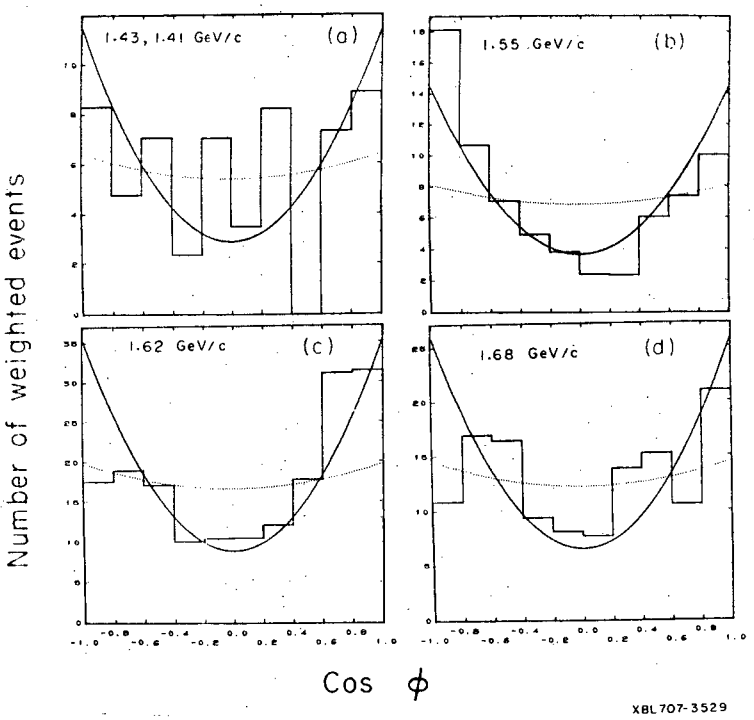

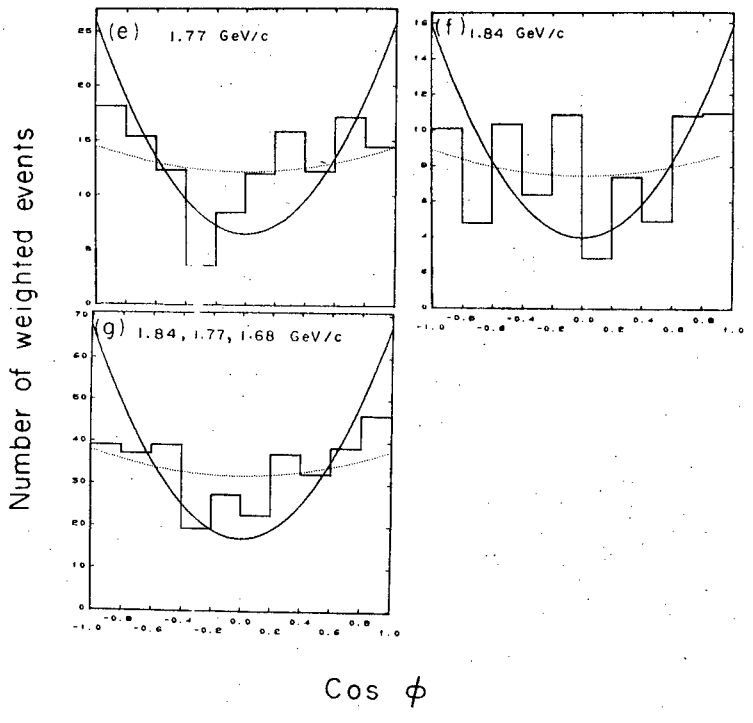

Fig. 7.

Decay angular distributions of the $Y^*(1385)$ with respect to the production normal. The angle ϕ is defined as being the angle in the Y^* c.m. between the production normal ($\hat{\pi}_{beam} \times \hat{K}^+$) and the decay π^+ from Y^*. The solid curve is the prediction from the Stodolsky-Sakurai model; the broken curve is the prediction assuming the reaction proceeds by $\pi^+ p \rightarrow \Delta(1950) \rightarrow Y^* K^+$ when the Δ decays via an $\ell = 3$ (not $\ell = 5$) state.

(a) π^+ momenta 1.41 and 1.43 GeV/c
(b) π^+ momenta 1.55 GeV/c
(c) π^+ momenta 1.62 GeV/c
(d) π^+ momenta 1.68 GeV/c
(e) π^+ momenta 1.77 GeV/c
(f) π^+ momenta 1.84 GeV/c
(g) π^+ momenta 1.68, 1.77, and 1.84 GeV/c combined.

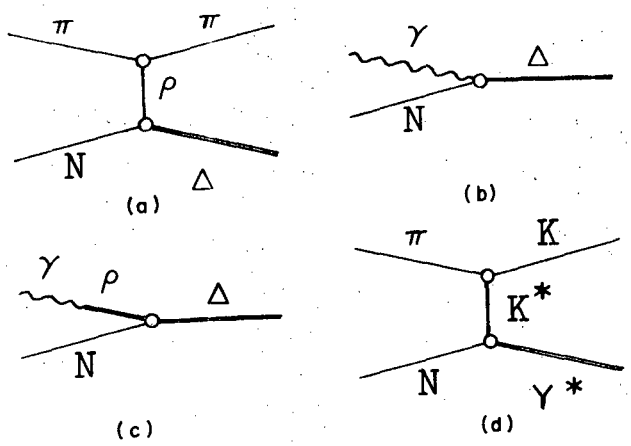

XBL707-3531

Fig. 8. Diagrams for (a) Δ production by ρ exchange; (b) photoproduction of a Δ; (c) photoproduction of a Δ mediated by ρ meson (rho-photon analogy); (d) $Y^*(1385)$ production by $K^*(890)$ exchange.

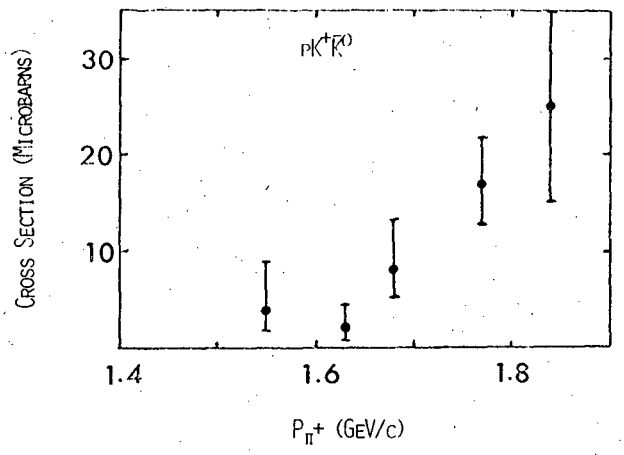

XBL707-3532

Fig. 9. Cross sections for the channel $\pi^+ p \rightarrow pK^+\bar{K}^0$.

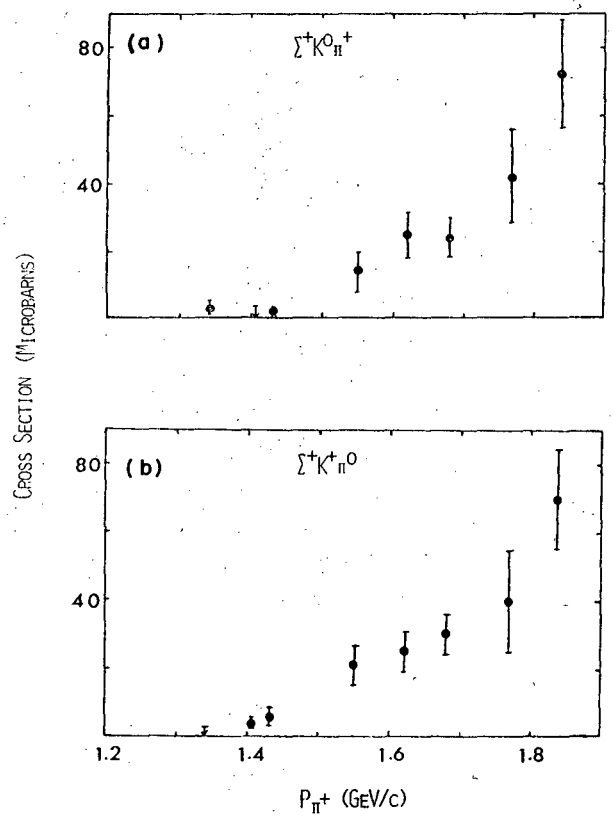

XBL707-3533

Fig. 10. Cross sections for the channels $\pi^+ p \rightarrow \Sigma^+ K^0 \pi^+$ and $\pi^+ p \rightarrow \Sigma^+ K^+ \pi^0$.

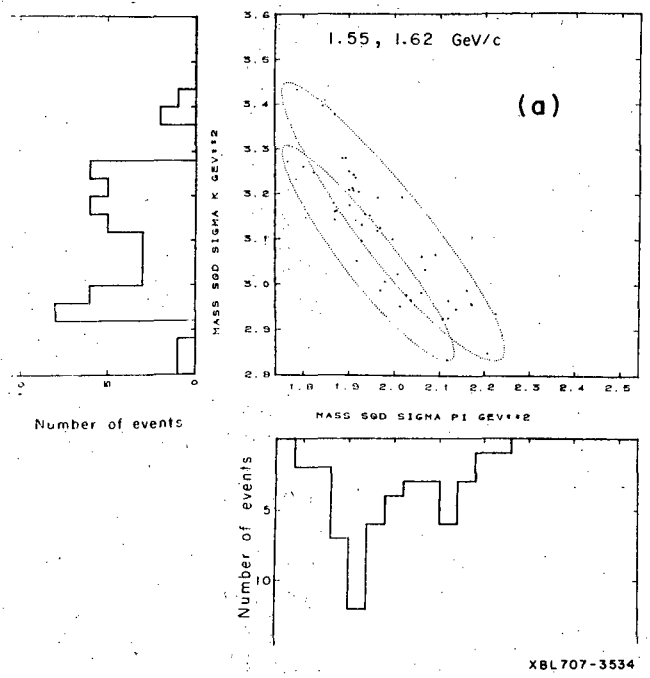

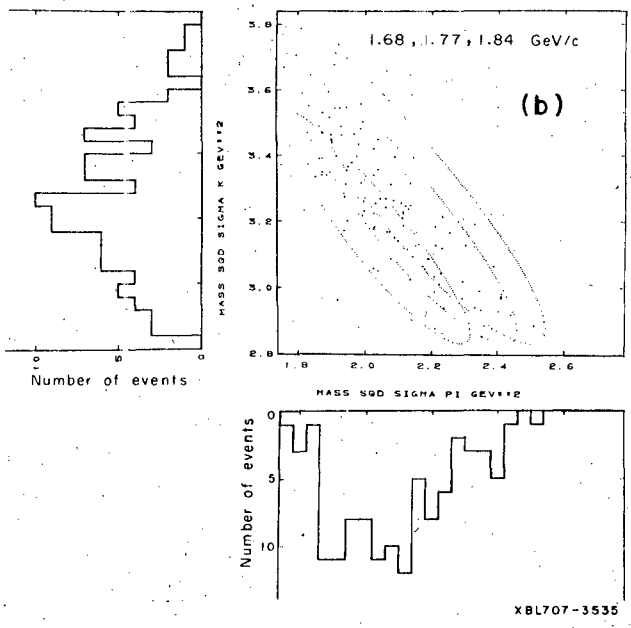

Fig. 11. Plots of Σ^+K^+ invariant mass squared versus $\Sigma^+\pi^0$ invariant mass squared and histograms of the projections onto the two axes.
(a) π^+ momenta 1.55 and 1.62 GeV/c combined
(b) π^+ momenta 1.68, 1.77, and 1.84 GeV/c combined

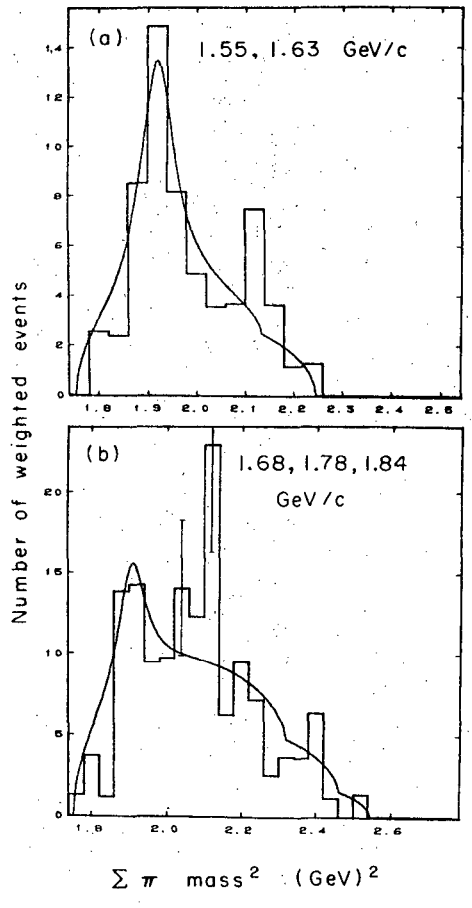

Fig. 12. $\Sigma^+\pi^0$ invariant mass squared histogram for weighted events.
(a) 1.55 and 1.62 GeV/c
(b) 1.68, 1.77, and 1.84 GeV/c

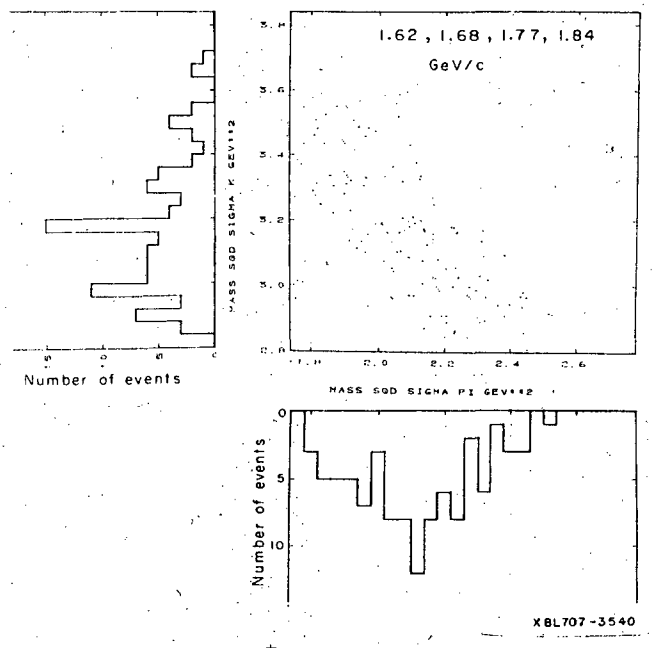

Fig. 17. Plot of Σ^+K^0 invariant mass squared versus $\Sigma^+\pi^+$ invariant mass squared and histograms of the projections onto the two axes for the 1.62-, 1.68-, 1.77-, and 1.84 GeV/c data combined.

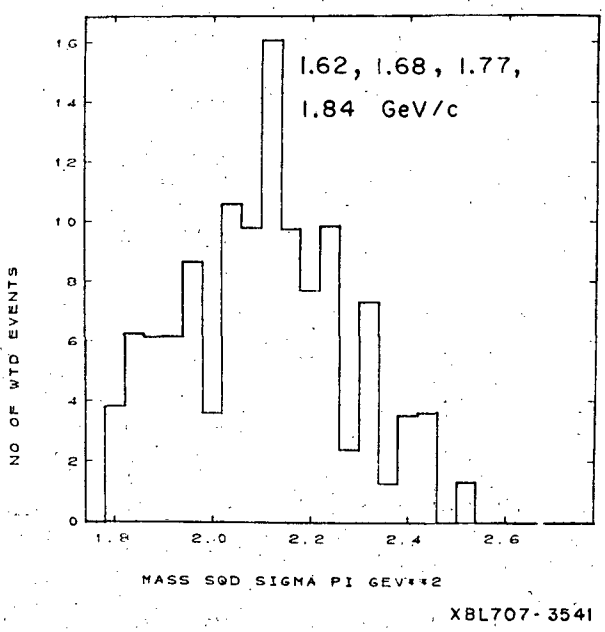

Fig. 18. Histogram of the $\Sigma^+\pi^+$ invariant mass squared for weighted events: 1.62-, 1.68-, 1.77-, and 1.84 GeV/c data combined.

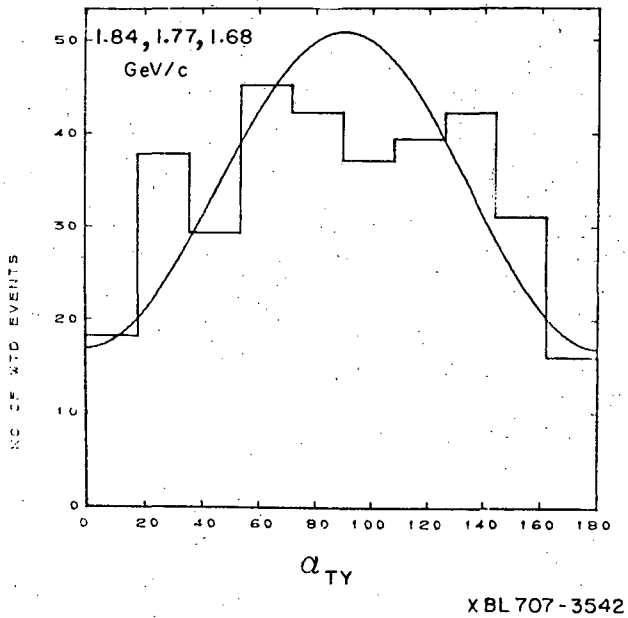

Fig. 19. Treiman-Yang angle for the Y^* decay. The curve is the prediction for the Stodolsky-Sakurai model (1.68-, 1.77-, and 1.84-GeV/c data combined).

LEGAL NOTICE

TECHNICAL INFORMATION DIVISION
LAWRENCE RADIATION LABORATORY
UNIVERSITY OF CALIFORNIA
BERKELEY, CALIFORNIA 94720